JOURNAL OF GEOPHYSICAL RESEARCH, VOL. 99, NO. C4, PAGES 7787–7802, APRIL 15, 1994

Backscatter characteristics of the winter ice cover in the Beaufort Sea

Ronald Kwok and Glenn F. Cunningham
Jet Propulsion Laboratory, California Institute of Technology, Pasadena

Abstract. The microwave backscatter statistics of the sea ice cover in the winter Beaufort Sea are characterized using C band synthetic aperture radar (SAR) data collected by the European Earth Resources Satellite 1. Sea ice backscatter signatures were sampled from SAR image data collected during the winter of 1991–1992 and winter of 1992–1993. The spatial and temporal variabilities of the backscatter signatures of different ice types are discussed. The results show considerable seasonal stability of the backscatter signature of multiyear ice as well as of first-year ice. Small amplitude regional variations of the multiyear ice backscatter can be observed. Consistent contrast between multiyear ice and first-year ice is maintained throughout the season. The highest radiometric variability is observed in sea ice in leads. On the basis of these observations the backscatter from the principal ice types (multiyear and first-year) are consistent with scatterometer observations and can be easily identified under winter conditions. Correlations of the regional variations of multiyear ice signatures to physical processes are suggested.

1. Introduction

The spatial and temporal coverage of the European Earth Resources Satellite 1 (ERS-1) synthetic aperture radar (SAR) provide an opportunity to systematically monitor the regional and seasonal behavior of the backscatter signatures of sea ice from a spaceborne sensor. The effective retrieval of ice type information from radar data is dependent on the uniqueness of these radar signatures as well as on their quantitative description. Numerous studies (e.g., summarized by *Ulaby et al.* [1986]) [*Onstott et al.*, 1979, 1982; *Kim et al.*, 1985; *Livingstone and Drinkwater*, 1991; *Gray et al.*, 1982] during recent years have investigated the dependence of sea ice backscatter on frequency, incidence angle, and polarization. These ice signatures also vary significantly with seasonal temperature variations [*Onstott and Gogineni*, 1985; *Onstott et al.*, 1987; *Holt and Digby*, 1985; *Livingstone et al.*, 1987a; *Carsey*, 1985; *Cavalieri et al.*, 1990; *Livingstone et al.*, 1987b]. Several recent studies have compared theoretical scattering models based on ice properties to the observed radar ice signatures [*Drinkwater et al.*, 1991; *Winebrenner et al.*, 1989; *Drinkwater*, 1989; *Kim et al.*, 1985]. These studies include in situ, laboratory, and aircraft measurements with some coordinated ground support. They have demonstrated that sea ice types have well-defined radar-scattering signatures under certain environmental conditions. Indeed, algorithms [*Lyden et al.*, 1984; *Wackerman et al.*, 1988; *Shokr*, 1991; *Kwok et al.*, 1992] have been developed to utilize these frequency and polarization diverse measurements for identification of ice types in remote sensing data. While these studies are useful for obtaining fundamental knowledge about the scattering properties of sea ice, the areal coverage has usually been very sparse and the observation periods too limited to permit good spatial and temporal characterizations of the scattering signature of the sea ice cover. The regional dependence of ice signatures derived from spaceborne radar data is not well known.

The purpose of this work is to provide a more extended study of the C band (5.3 GHz) VV (vertically polarized transmit/vertically polarized receive) backscatter signature of sea ice in the winter Beaufort Sea using data collected by the ERS-1 SAR. The spatial and temporal characterization of ice signatures also enables the evaluation of the statistical variability of sea ice backscatter. Here we use the seasonal descriptors suggested by *Livingstone et al.* [1987b] and restrict our sampling to only winter conditions when typically there is a dry snow pack overlying dry cold ice with air temperatures that are less than −10°C. In this study we characterize the microwave signature of the sea ice cover in the Beaufort Sea during the winters of 1991–1992 and 1992–1993 based solely on observations derived from SAR data. Such characterizations are important when a unique set of signatures for each ice type are required for the eventual extraction of information from satellite data.

Under cold dry winter conditions it has been observed that there is significant contrast between multiyear ice and first-year ice when the probing frequency is C band or higher. The significance of particular sea ice characteristics and their effects on microwave backscatter was summarized in *Winebrenner et al.* [1989]. The relatively higher contribution of the multiyear ice volume, compared to the ice surface, to the scattering process is the generally accepted physical explanation for the observed contrast in backscatter. In sea ice, as in most natural media, electromagnetic scattering takes place from inhomogeneities within the volume of the medium, from irregular surfaces bounding the medium, or from both. The fundamental difference between backscatter from first-year and multiyear ice is the higher salinity of the former. The superimposed dry snow layer does not significantly affect the observed backscatter at C band [*Kim et al.*, 1985]. For a given surface roughness, then, the contribution

Paper number 94JC00169.
0148-0227/94/94JC-00169$05.00

to the scattering cross section from these inhomogeneities (air bubbles, brine pockets) in the multiyear ice is much higher because of the low salinity in the ice layer. The signature dynamics of younger and thinner ice types, however, are more complex and less well defined from a uniqueness point of view. The characterization of these signatures, which is not readily done in ERS-1 SAR imagery, is more involved and is not treated in this study. The calibration of the ERS-1 SAR is reviewed in section 2. We describe our approach to spatial and temporal sampling of the sea ice signatures in section 3. The multiyear, first-year, and lead ice type signature records are summarized in sections 4 and 5. Summary remarks are provided in section 6.

2. Data Calibration and Characteristics

The data used in this study were collected by the ERS-1 synthetic aperture radar. The sensor is a C band (5.3 GHz) radar operated with vertical transmit and receive polarizations at a look angle of 20°. Within the antenna beam, which illuminates a swath of approximately 100 km in width, the incidence angles on the ground vary from 19° at near range to almost 26° at far range. The image data used in this study were received and processed at the Alaska SAR Facility (ASF) in Fairbanks, Alaska. Each image frame covers an area of approximately 100 km by 100 km. The SAR processor at ASF produces full resolution ground plane data which is sampled at 12.5 m. The data type used in this study is a lower-resolution image product created by increasing the sample spacing to 100 m by the averaging of 8 × 8 full resolution pixel samples. The lower-resolution data was selected because of the lower speckle content of the data. If the high-resolution products were used, the speckle would introduce a bias in the observation of the second moments of the backscatter statistics. One limitation of lower resolution is that smaller leads are not sampled in our data collection process. Ancillary data are provided with each image frame for calibration and conversion of the eight-bit digital data into normalized backscatter cross sections.

Calibration of the radar is measured in an absolute and relative sense. The absolute calibration accuracy metric quantifies the uncertainty of a measured normalized backscatter cross-section (σ_0) measurement relative to the actual σ_0 of a distributed target. Typically, this appears as a bias when an identical target from two image frames (imaged at different times) are compared. The in-scene variance of a target known to have uniform backscatter cross section is measured by the relative calibration accuracy. Relative calibration is usually better than absolute calibration and is easily maintainable, especially if the radar sensor is stable. The data products used in this study have expected absolute and relative accuracies of 2 dB and 1 dB, respectively [*Fatland and Freeman*, 1992]. The noise equivalent σ_0 of the ERS-1 radar data is at approximately −24 dB, which means that the backscatter power from a distributed target with a σ_0 of −24 dB is equivalent to the noise power of the sensor. The detectability of such backscatter targets is therefore limited by this quantity. We note here that low-backscatter sea ice (e.g., grease ice) in the incidence angle range of ERS-1 could be less than −30 dB and is therefore in theory radiometrically undetectable within the dynamic range of the data. The above factors provide the limits to the observations made here. Because of the expected range of backscatter first-year and multiyear ice, the observations of their temporal and regional backscatter characteristics should not be significantly affected by these factors.

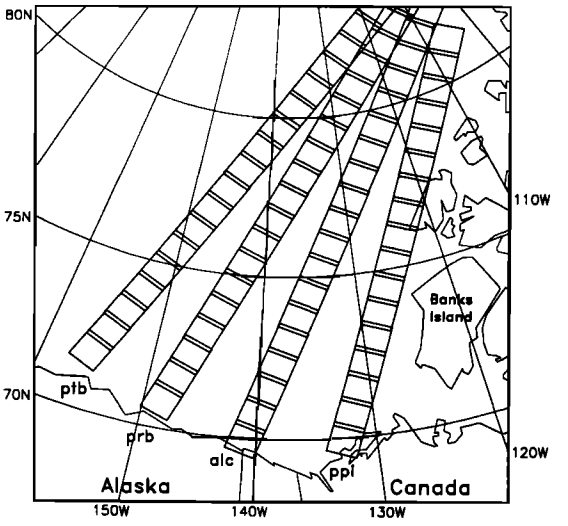

Figure 1. Coverage of the four descending ERS-1 tracks (within the ASF mask) during the ice phase.

3. Data Analysis Approach

The region studied in this paper is shown in Figure 1. A first data set was obtained from data collected during the 3-day repeat cycles of the ERS-1 commissioning and ice phases. There were four descending SAR tracks which covered a region bounded on the south by the Alaskan and Canadian coasts, on the east by Banks Island and Prince Patrick Island, and on the west by a line running from 70°N, 160°W to approximately 83°N, 135°W. The commissioning phase lasted from August 6 through December 9, 1991, while the ice phase lasted from December 28, 1991, through April 2, 1992, after an 18-day orbit adjustment period between phases. This first data set provided us with a temporal record of ice signatures spanning six winter months from October 1991 through March 1992. The second smaller data set was obtained from data collected from similar descending tracks during the multidisciplinary phase (35-day repeat) in the months of November and December of 1992. These two data sets provide us with a comparison of winter ice signatures of the sea ice cover for two consecutive winters. The data presented in the following sections are labeled and organized by these four tracks, designated hereafter by the land boundaries they intersect: ptb, Point Barrow; prb, Prudhoe Bay; alc, Alaskan/Canadian border; and ppi, Prince Patrick Island. These orbit tracks allow us to sample the character of the similar ice types near the Canadian Archipelago, the Alaska Coast, the central and western Beaufort Sea and the central Arctic.

Samples for signature characterization were extracted from images when the air temperature was below −10°C at the time of acquisition. Under these winter conditions, when the typical observed scattering configuration is cold dry snow over an ice layer, the temperature modulation of the backscatter should be small. This ensures that the collected statistics are not contaminated by mixtures of ice and ice with surface melt. Figure 2 shows the region-wide air tem-

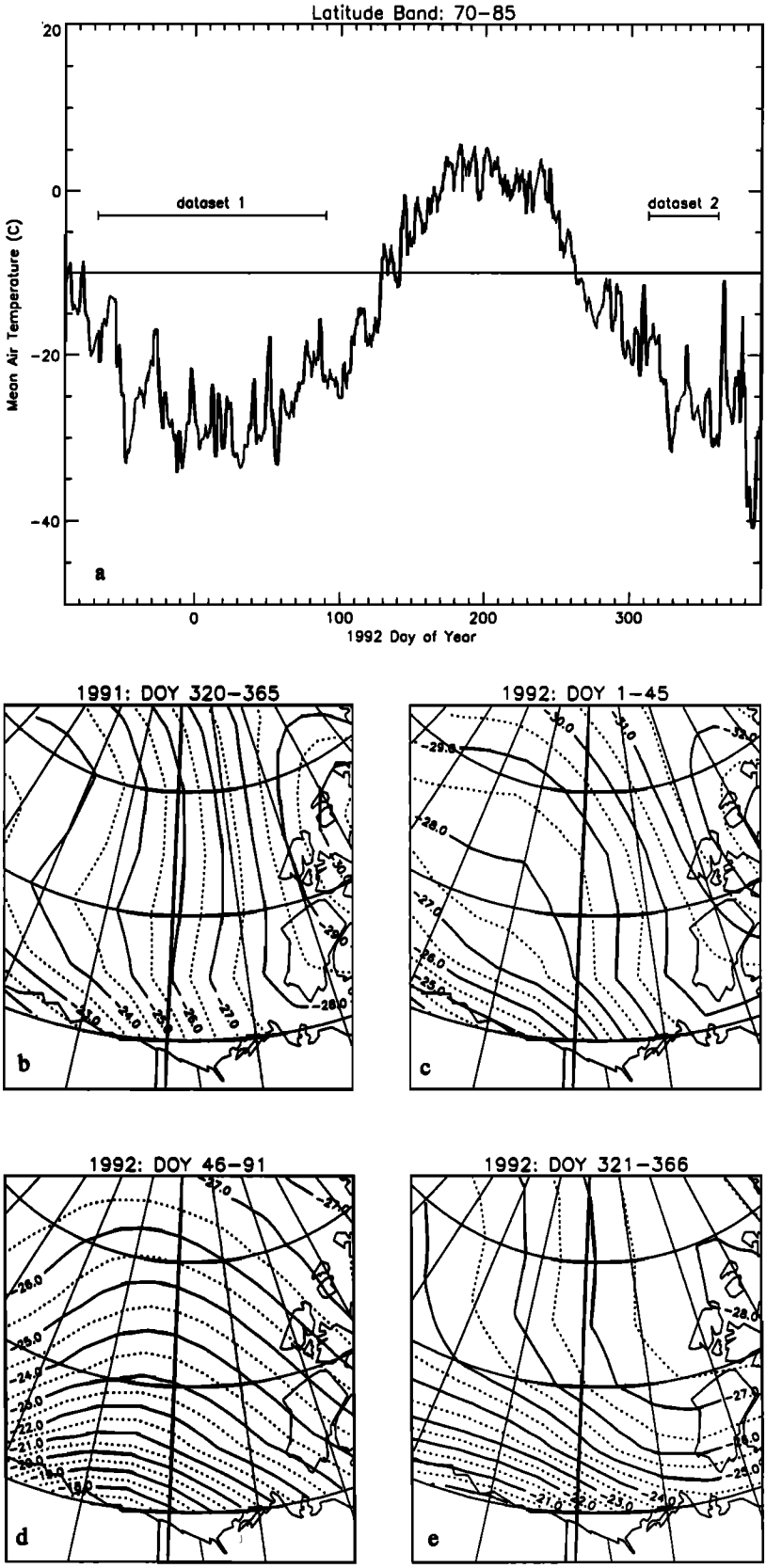

Figure 2. Region-wide 1000-mbar air temperature record (in degrees Celsius). For convenience, the abscissa is plotted as 1992 day-of-year (DOY), using negative values during 1991. (a) Region-wide temperature record. (b) Averaged temperature distribution 1991, DOY 320–365. (c) Averaged temperature distribution 1992, DOY 1–45. (d) Averaged temperature distribution 1992, DOY 46–91. (e) Averaged temperature distribution 1992, DOY 321–366.

Table 1. Times and Numbers of Sampled Images

ptb		prb		alc		ppi	
DOY	No. of Images	DOY	No. of Images	DOY	No. of Images	DOY	No. of Images
...	...	299	11	297	19	...	...
310	3	311	15	309	12	...	...
322	14	323	2	321	3	...	...
334	15	335	15	339	16	...	...
5	12	6	17	4	11	...	...
17	18	18	18	16	20	17	17
29	17	...	...	...	...	29	17
41	17	42	17	...	...	...	...
53	17	...	...	52	19	53	17
65	19	66	20	...	...	...	...
77	19	78	20	76	19	...	...
89	19	90	20	88	18	89	17
312	12	313	16	314	14	315	8
359	18	360	17	364	18	359	10
Total	200	Total	188	Total	169	Total	86

DOY, day of year. A total of 643 images were used.

perature record over the Beaufort Sea during the period of interest. This air temperature time series was derived from gridded (2.5° latitude by 5° longitude grid) every 12 hours National Meteorological Center (NMC) 1000-mbar air temperature analyses. While these temperatures may not represent the actual physical surface air temperature due to uncertainty in the NMC analyses (typically the temperature fields are biased due to difficulty in modeling the inversion layer), they are nevertheless indicators of the winter conditions predicated in this study. The data show that the region-wide average temperature stayed below −10°C starting around day of year (DOY) 313 or November 9, 1991. Temperatures at actual SAR image center times and locations show that all but five images were acquired when the temperature was below −10°C.

Because of the large number of SAR image products which were available over the four tracks, a spatial and temporal sampling strategy was utilized and is described below. The tracks were sampled every 12 days in the first data set. In the second data set, the four tracks were each sampled once over a period from late November through early December. Table 1 summarizes the temporal and spatial coverage of the two datasets. The DOY and number of images sampled are given for each orbit. A gap in the table indicates that images for that time had not been processed by ASF at the time of this study. In all, more than 600 images were used in this study.

Figure 3 shows an ERS-1 sea ice image from the winter Beaufort Sea. The higher-backscatter multiyear ice can easily be discriminated from the other ice types. Upon closer examination, at least 2–3 other ice types can be identified (using their backscatter intensities). In this study, sample windows were visually classified as one of five ice types from the perennial ice zone (PIZ) and the seasonal ice zone (SIZ). The rationale for this classification is the relative ease with which samples can be visually identified. It should be noted here that because of the disparity between the resolution of typical land-based scatterometer and spaceborne SAR observations, it is expected that SAR image backscatter observations are modulated to a higher degree by mixtures of ice types and deformation features compared with scatterometer observations of pure ice types. It is expected that observations at the larger scale (larger areal extent) could be biased or have larger variance in backscatter than the pure ice type. The image statistics were collected and the samples labeled as one of five sea ice types using knowledge of their spatial context and backscatter intensity. The ice types and the limitations of visual identification of them are discussed as follows:

1. Deformed multiyear ice (MY-D) is multiyear ice which includes deformed features, i.e., all ridges, hummocks, or surface topography which give a textured appearance to the imagery. This ice type may include deformed first-year rubble that has frozen into multiyear (MY) floes [*Rignot and Drinkwater*, 1994], although the average fractional area coverage of this first-year rubble on MY floes has not been measured. The σ_0 of this ice type is generally higher than that of undeformed multiyear ice.
2. Undeformed MY ice (MY-U) is multiyear ice with smooth texture and appearance with no obvious large-scale ridging or deformation.
3. Deformed first-year ice (FY-D) is FY ice in the SIZ with deformed features due to ridging and rafting. This classification allows us to characterize the variability of the FY ice signature, especially of ice in the shear zone.
4. Undeformed FY ice (FY-U) is FY ice in the SIZ with smooth texture and appearance with no obvious deformation features.
5. Lead ice in the PIZ is ice that appears in cracks, fractures, and openings in the ice pack (PIZ). This ice could be in various stages of growth. Our definition of a "lead" is more of a geometric definition and is a feature which appears as a crack or fracture in the ice. It includes ice (e.g., new, young, grease, frazil, pancake, etc.) or open water with high and low backscatter. This classification allows us to monitor the backscatter variability of ice in the leads. We do not include leads with high backscatter because of the difficulty in sampling these pixels and because of the ambiguity of the

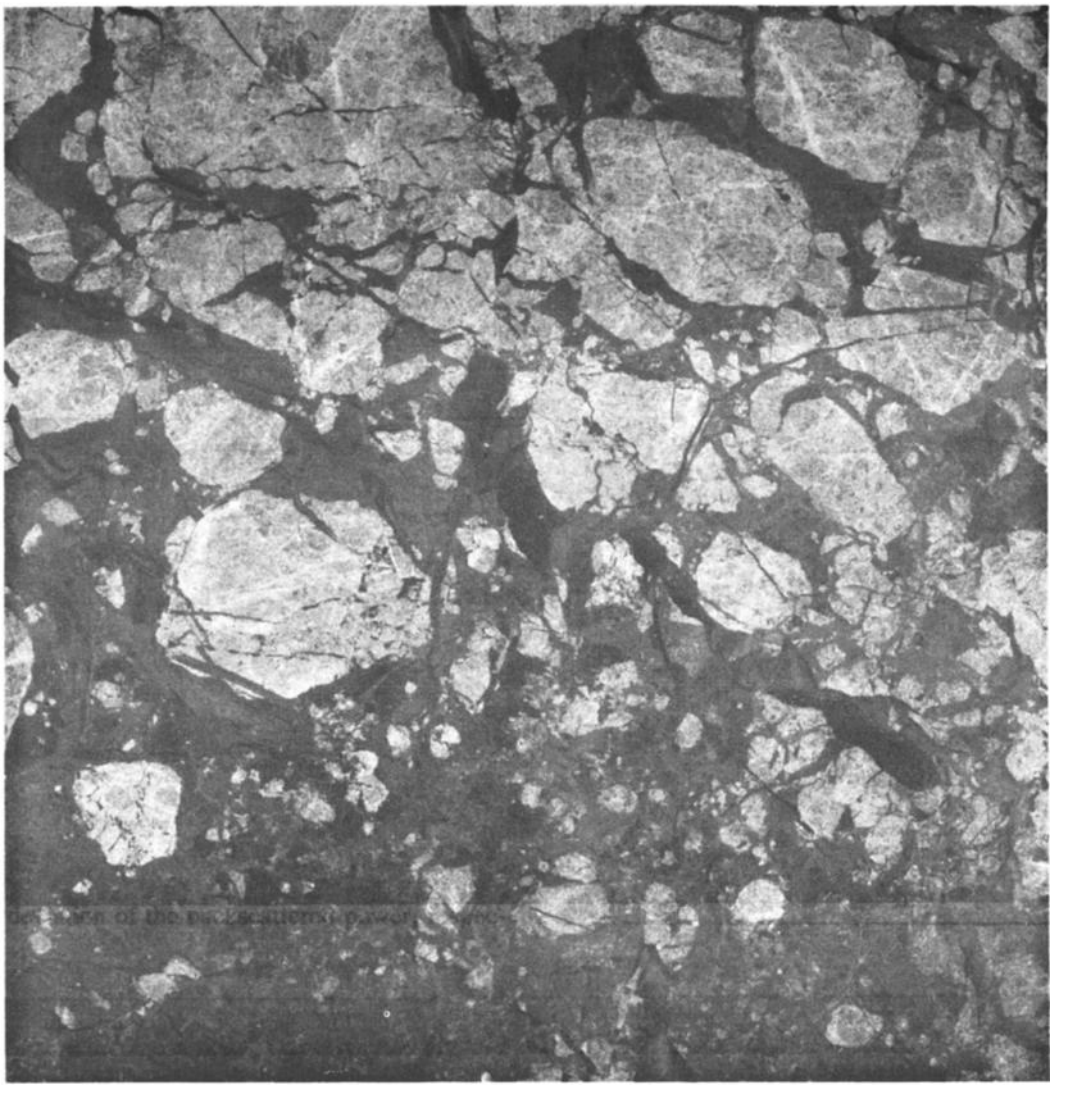

Figure 3. ERS-1 SAR image showing sea ice in the Beaufort Sea on November 27, 1991, at 72.3°N, 153.3°W (Copyright ESA 1992).

signature of this ice type compared with the signature of MY and deformed FY ice.

The sampling method consisted of interactively defining an area on the SAR image with an arbitrary polygon. Wherever possible, large sample populations were chosen to increase the confidence in the estimation of the backscatter statistics. Typically, sample sizes varied from around 30 pixels (0.3 km^2) in small, narrow leads to 3000 pixels (30 km^2) for samples collected over large multiyear floes. Summary statistics (mean and standard deviation) of the backscatter and incidence angle for each sample window were recorded. There are a number of ways to represent the standard deviation (in decibels) on a logarithmic scale. In this paper we define the standard deviation (in decibels) as follows:

$$S.D.(\text{dB}) = 10 \log \frac{P_0 + P_{S.D.}}{P_0}$$

where P_0 and $P_{S.D.}$ are the mean backscattered power and the standard deviation of the backscattered power, respectively. Tables 2 and 3 give the number of samples taken for each ice class in each of the data tracks. The multiyear deformed (MY-D) and lead ice were most heavily sampled. The following sections provide discussions of the backscatter data set and their temporal and spatial variabilities.

4. Multiyear/Lead Ice Signature

In this section we discuss the regional, temporal, and incidence angle behavior of multiyear and lead ice signatures from the perennial ice zone.

Table 2. Number of Samples for Each Ice Type (Winter 1991)

	MY_D	MY_U	FY_D	FY_U	Lead
ptb	2677	205	152	126	885
prb	2480	371	57	113	858
alc	2317	300	26	96	804
ppi	1141	273	0	84	423
all	8615	1149	235	419	2969

Table 3. Number of Samples for Each Ice Type (Winter 1992)

	MY_D
ptb	411
prb	482
alc	449
ppi	180
all	1522

4.1. Multiyear (MY) Ice

The ERS-1 SAR is extremely stable, as evidenced by the consistency of multiyear ice backscatter signatures presented here. Thus even though there could be a bias in the observed backscatter cross section, the sensor and processor calibrations are such that the temporal variation of this bias is slow and small. The histograms of the backscatter of the deformed and undeformed MY samples in Figure 4 show that the two MY ice types differ only in the second moment. Owing to the relatively smaller number of undeformed multiyear ice samples and the similarity of the mean backscatter values of the two multiyear ice classes, only the deformed MY ice data are discussed here.

Spatial and temporal variability. The spatial and temporal variability of the backscatter signal of the deformed multiyear ice is summarized in Figure 5. The four columns represent the four data tracks while the four rows represent time averages of the backscatter. Orbit adjustment of the ERS-1 satellite was performed during the period DOY 340–365 in 1991 and thus the gap in the data sampling. Figure 6 uses contours to depict the spatial behavior of MY ice backscatter during these same time periods. Several general observations can be made about the data: (1) Backscatter from MY ice increases from the western Beaufort Sea to the Canadian Archipelago. (2) Above 75°N the backscatter of multiyear ice generally increases with latitude and is especially evident in the western Beaufort. There is a minima at around 75°N (in the western Beaufort) and the backscatter tends to increase toward the southern Beaufort. (3) The minimum and maximum of the sample means are almost all within 1 dB of the population mean. (4) At a given geographic location the multiyear ice backscatter remains quite stable (within 0.5 dB) throughout a given winter. (5) These same trends can be observed in the backscatter data from both winters.

We discuss each of these observations in more detail below. Before we attribute any physical significance to these observations, it is important to consider the limitations of the radar measurements. First, the latitude dependence of the backscatter seems to be a trend observed in the data set, and the change in most cases is approximately 2 dB. A sensor/processor effect could account for this observed trend because the ERS-1 SAR goes through almost identical thermal and Doppler histories (i.e., Doppler frequency due to the relative velocity of the phase center of the antenna and its illuminated area on the Earth) along these descending tracks, and therefore a systematic gain variation with latitude is possible. To test this hypothesis, the σ_0 of multiyear ice from two ascending and two descending pass image sets acquired within a 12-day period at four orbit-crossing points were sampled and compared (see Figure 7). The same trend is

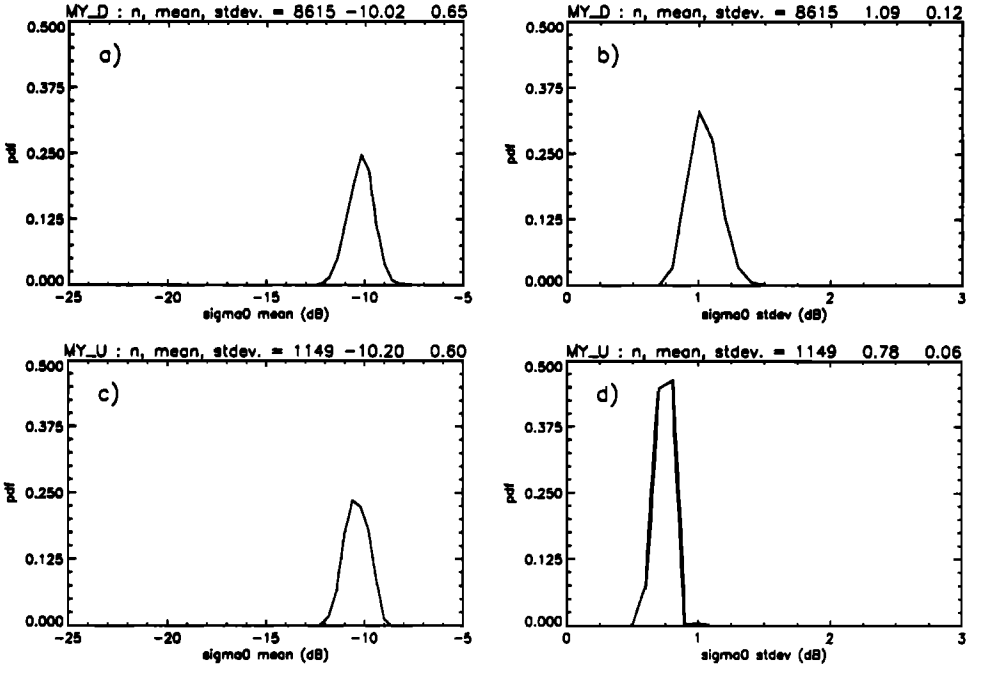

Figure 4. Histograms of mean and standard deviation of deformed MY (MY-D) and undeformed MY (MY-U) ice backscatter. (a) Mean backscatter of MY-D. (b) Standard deviation of backscatter of MY-D data samples. (c) Mean backscatter of MY-U. (d) Standard deviation backscatter of MY-U data samples. Binning intervals are 0.4 dB and 0.1 dB for the mean and standard deviation plots, respectively. (n = number of points in data set; mean = mean backscatter in decibels; stdev = standard deviation in decibels.)

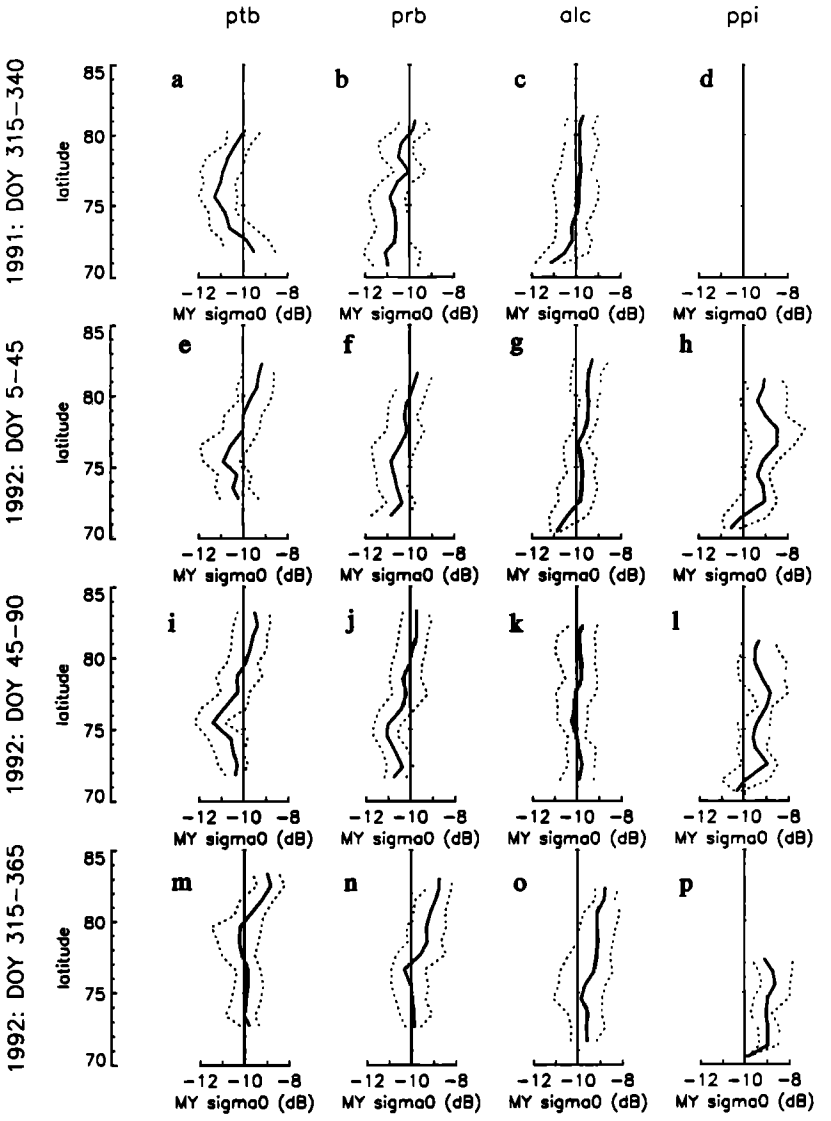

Figure 5. Spatial and temporal behavior of multiyear sea ice. The solid line in each plot shows the mean backscatter of all pixels within a 1° latitude bin plotted at their average latitude. The dotted lines show the minimum and maximum sample means found within that latitude bin. Bins are (a) ptb, 1991 DOY 315–340; (b) prb, 1991 DOY 315–340; (c) alc, 1991 DOY 315–340; (d) ppi, 1991 DOY 315–340; (e) ptb, 1992 DOY 5–45; (f) prb, 1992 DOY 5–45; (g) alc, 1992 DOY 5–45; (h) ppi, 1992 DOY 5–45; (i) ptb, 1992 DOY 45–90; (j) prb, 1992 DOY 45–90; (k) alc, 1992 DOY 45–90; (l) ppi, 1992 DOY 45–90; (m) ptb, 1992 DOY 315–365; (n) prb, 1992 DOY 315–365; (o) alc, 1992 DOY 315–365; (p) ppi, 1992 DOY 315–365.

observed in the ascending pass data, and the backscatter values were found to be consistent to within a few tenths of a decibel. Since the ERS-1 SAR encounters different thermal and Doppler histories in the ascending tracks, it is unlikely that the observations are sensor/processor induced. (The slightly higher difference between the ascending versus descending backscatter (0.4 dB) in the higher latitudes only enhances the trend and could be due to calibration uncertainties.)

Then, can such persistent features in the data be explained? Assuming we start with an initial latitude dependence in the backscatter data, does ice motion tend to randomize the observed trends? We consider the mean motion of the ice in the Beaufort Sea from October to March. The seasonal mean ice motion in the winter is an expression of the Beaufort Gyre with a magnitude of less than 2 cm/s (east to west motion) near 75°N generally decreasing with latitude [*Colony*, 1990], i.e., northward toward the center of the gyre. With an average ice motion of 2 cm/s, the total ice motion over the period of interest (approximately 160 days) over the Beaufort Sea is approximately 270 km, or a few SAR image frames. It is not surprising then that such persistence can be observed in the data.

Along the ppi tracks (see Figures 5 and 6) which sample the MY ice near the Canadian Archipelago, the MY ice shows generally higher backscatter values with two backscatter maxima near the location of Prince Patrick Island near 77°N and Banks Island near 73°N. The higher backscatter is probably due to the age and deformation of the ice in this region due to convergence of ice causing extensive

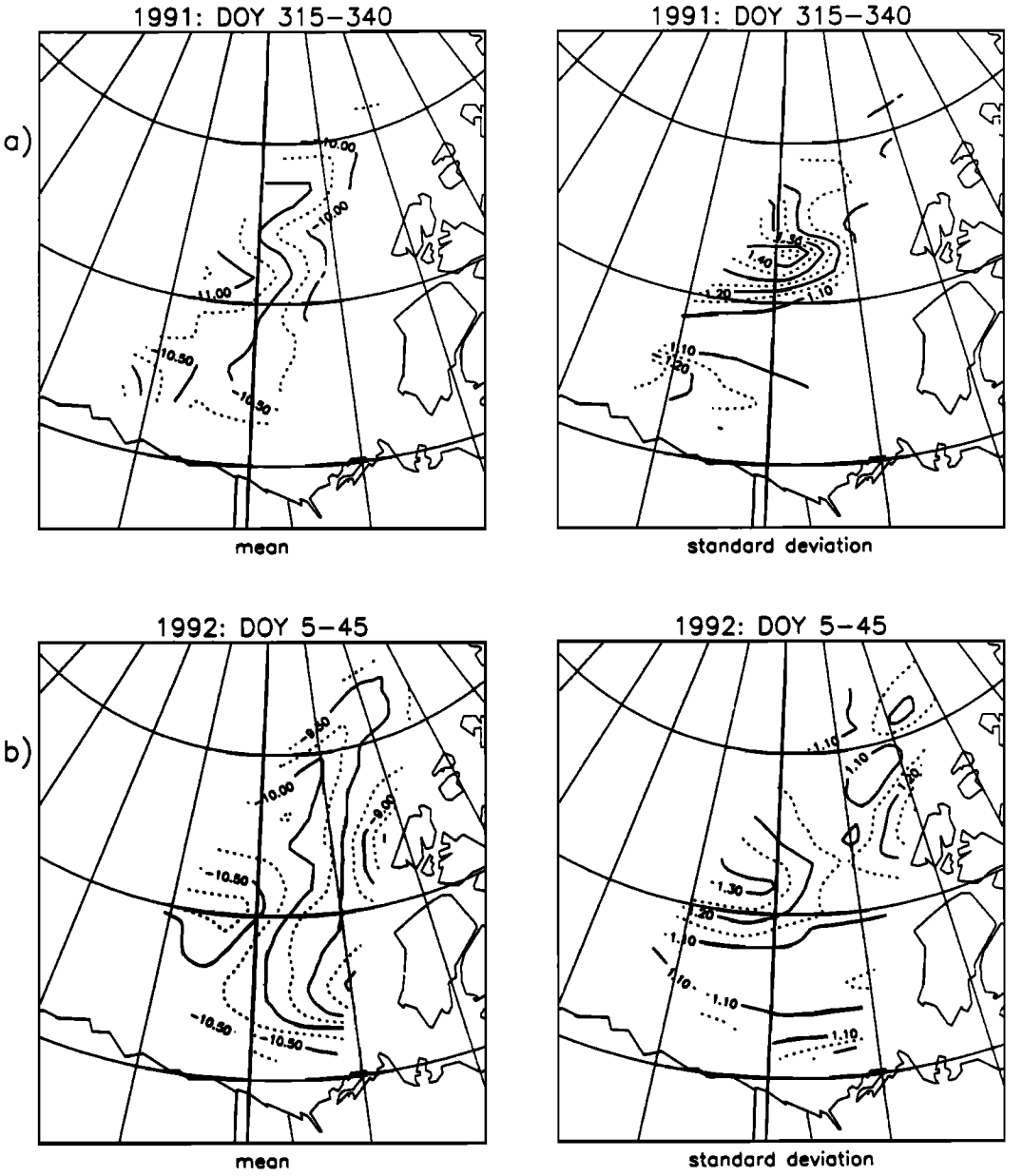

Figure 6. Spatial contours of mean and standard deviation of MY backscatter data from winter of 1991–1992 (1991 DOY 315 through 1992 DOY 90) and winter of 1992 (1992 DOY 315–365). (a) DOY 315–340, 1991. (b) DOY 5–45, 1992. (c) DOY 45–90, 1992. (d) Winter of 1991–1992. (e) Winter of 1992 (DOY 315–365, 1992).

pressure ridging of the ice cover. We observed that the SAR images show that the MY floes have different appearances than the floes in the western Beaufort Sea, as seen in the two images of Figure 8. There are more ridges in the image in the eastern Beaufort. Comparison of the spatial backscatter contours with mean ice thickness and age contours of the sea ice [*Bourke and McLaren*, 1992; *Colony and Thorndike*, 1985] show correlation of these data sets near the Canadian Archipelago and in the other parts of the Beaufort Sea. The thickness and age near the archipelago is twice the basin-wide mean age and thickness. This provides evidence that the deformation (e.g., hummocks, ridges, etc.) in the MY ice due to the mechanical processes in this region is responsible for the observed backscatter contrast between MY ice in this region and the other parts of the Beaufort Sea. We also observe (Figures 6b and 6c) the westward advection of the higher-backscatter contours most probably due to the transport of the thicker, more deformed or higher-backscatter MY sea ice from the Canadian Archipelago to the western Beaufort.

We offer speculations as to the physical significance of the latitude dependence observed in the western Beaufort. The MY backscatter in this region is generally lower than that observed near the Canadian Archipelago, with the general backscatter increasing with latitude. From a microscopic ice characteristics point of view, the salinity, air bubbles, and temperature are the most important factors which affect the backscatter of multiyear ice. Multiyear ice has a fairly

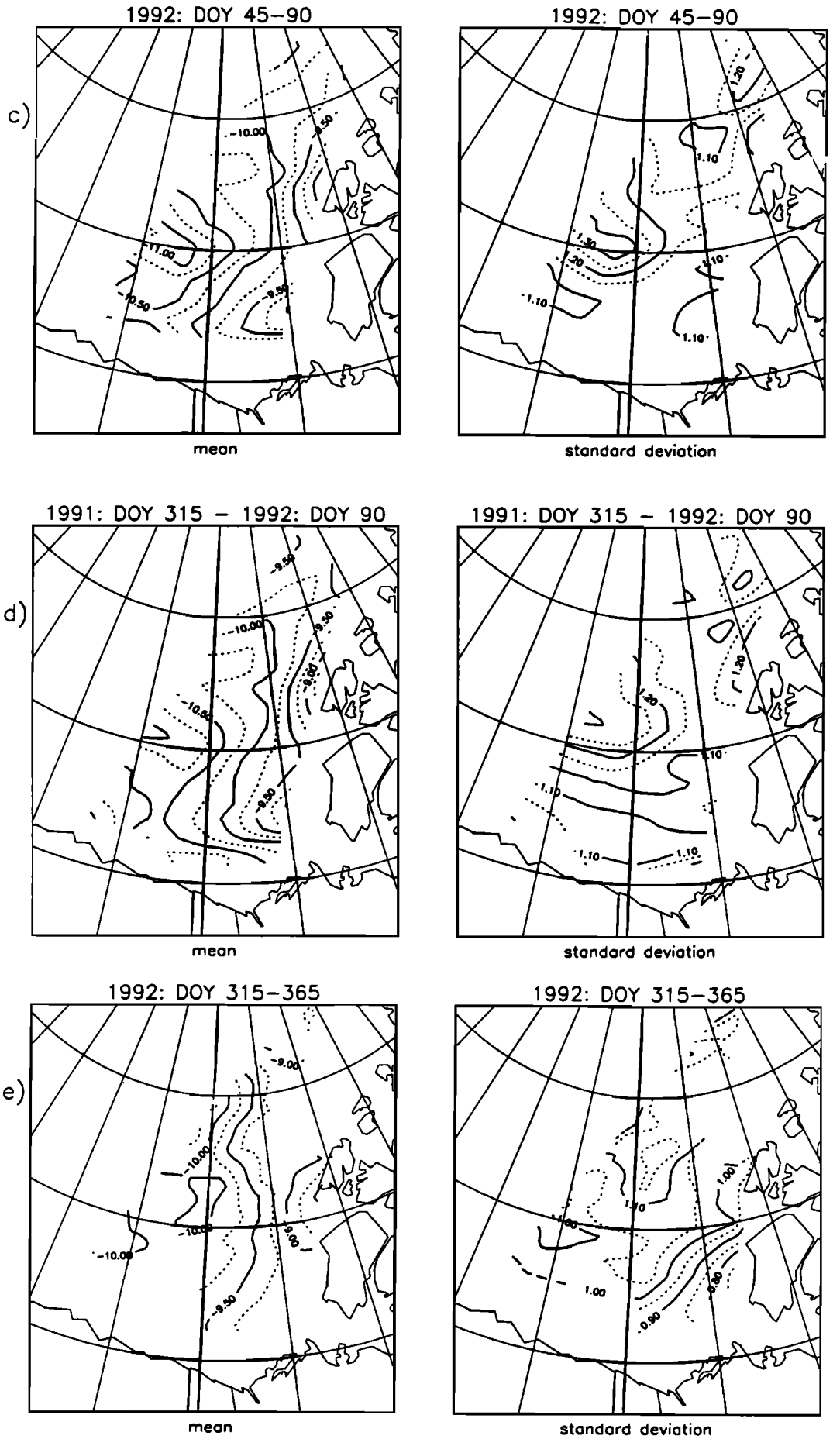

Figure 6. (continued)

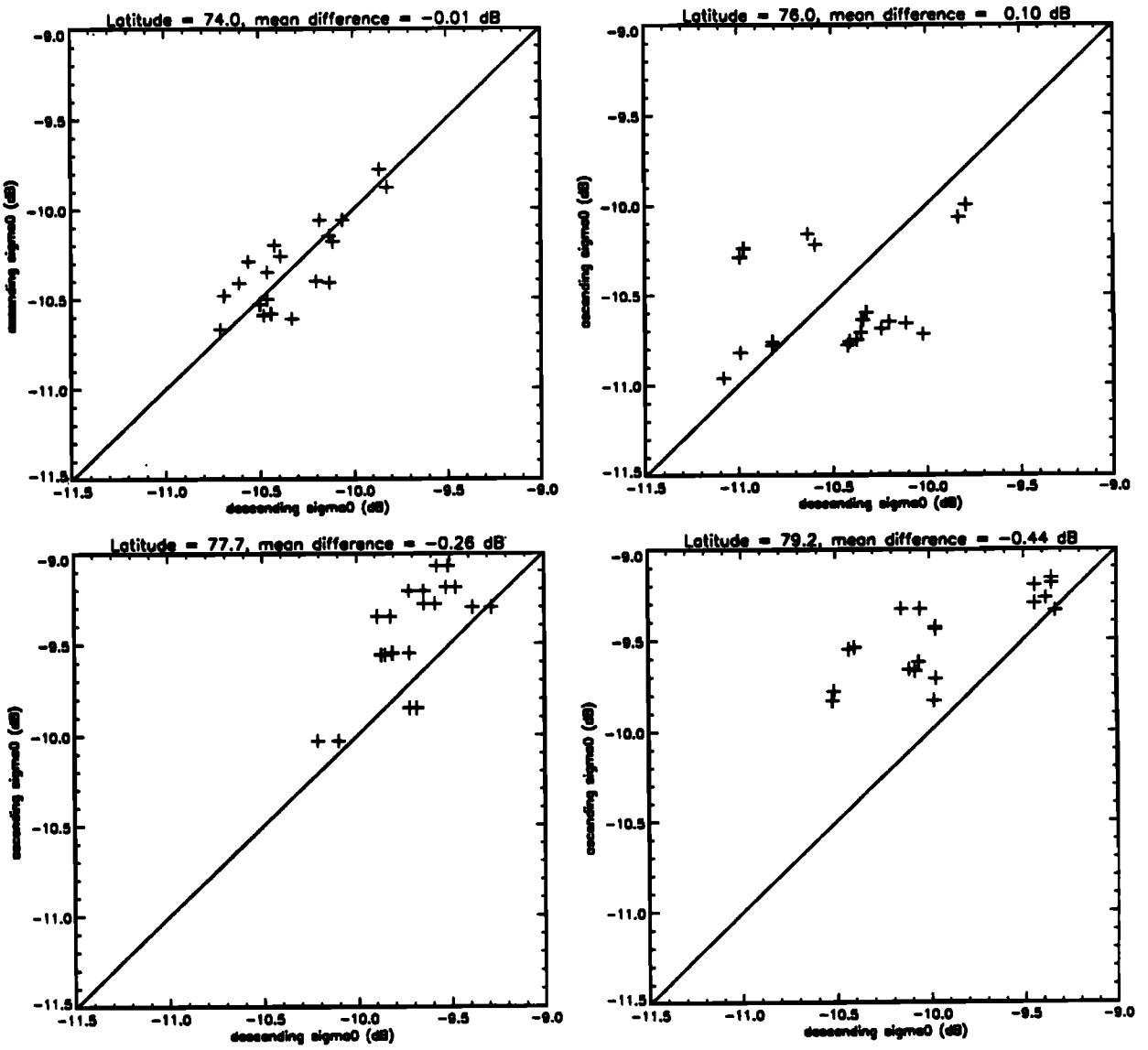

Figure 7. Comparison of MY samples taken from overlapping ascending and descending passes at four different latitudes. The mean difference is shown with each figure. (Each point represents a distinct floe sampled in both images.)

narrow range of salinity and is typically less than 2 parts per thousand (ppt) [*Gow et al.*, 1987]. With salinity alone, it takes a rather large change in salinity of 3 ppt to explain a 1.5 dB difference in the backscatter (S. V. Nghiem, personal communication, 1992). Thus it seems difficult to attribute the observation to a salinity effect. Variations in the size of air bubbles could certainly affect the backscatter, but we do not have any current evidence that size distribution is dependent on geographic location. Backscatter variation due to thermal modulation is probably small under the winter conditions considered here. On a larger scale, over the areal extent of the sample windows used to calculate the mean backscatter, the measurement represents backscatter contributions from frozen melt ponds, undeformed, and deformed (e.g., ridges, hummocks, etc.) ice features all of which are not resolved at the resolution of the data product used. A higher fractional area in frozen melt ponds tends to decrease the overall backscatter, whereas higher fractional areas of deformed features tends to enhance backscatter. If the basin-wide mean thickness of the ice away from the islands is approximately the same [*Bourke and McLaren*, 1992], then the degree of melt-ponding on multiyear floes can more likely explain the backscatter differences of the magnitude observed here. In the preceding statement we assume that deformation is correlated with mean thickness. Ponding on old ice occupies between 25–45% of the surface [*Carsey*, 1985]. If the σ_0 of multiyear ice was −10 dB and that of multiyear ice with superimposed frozen melt ponds was −20 dB [*Onstott*, 1992], a 20% decrease in areal coverage of refrozen melt ponds can account for the higher backscatter observed at higher latitudes (assuming a linear contribution of backscatter power from MY ice and frozen ponds). There is little observational literature on fractional frozen melt pond coverage of multiyear ice in the winter Arctic. It seems more likely that the effect is a combination of fractional melt pond coverage and deformation, although there are insufficient field observations to resolve this hypothesis at this time.

Figure 8. ERS-1 SAR images o n February 22, 1992. (a) The eastern Beaufort (image center location 78.0°N, 119.5°W; average σ_0 of image = −10.7 dB). (b) The western Beaufort (image center location 77.6°N, 145.5°W; average σ_0 of image = −8.9 dB). (Copyright ESA 1992)

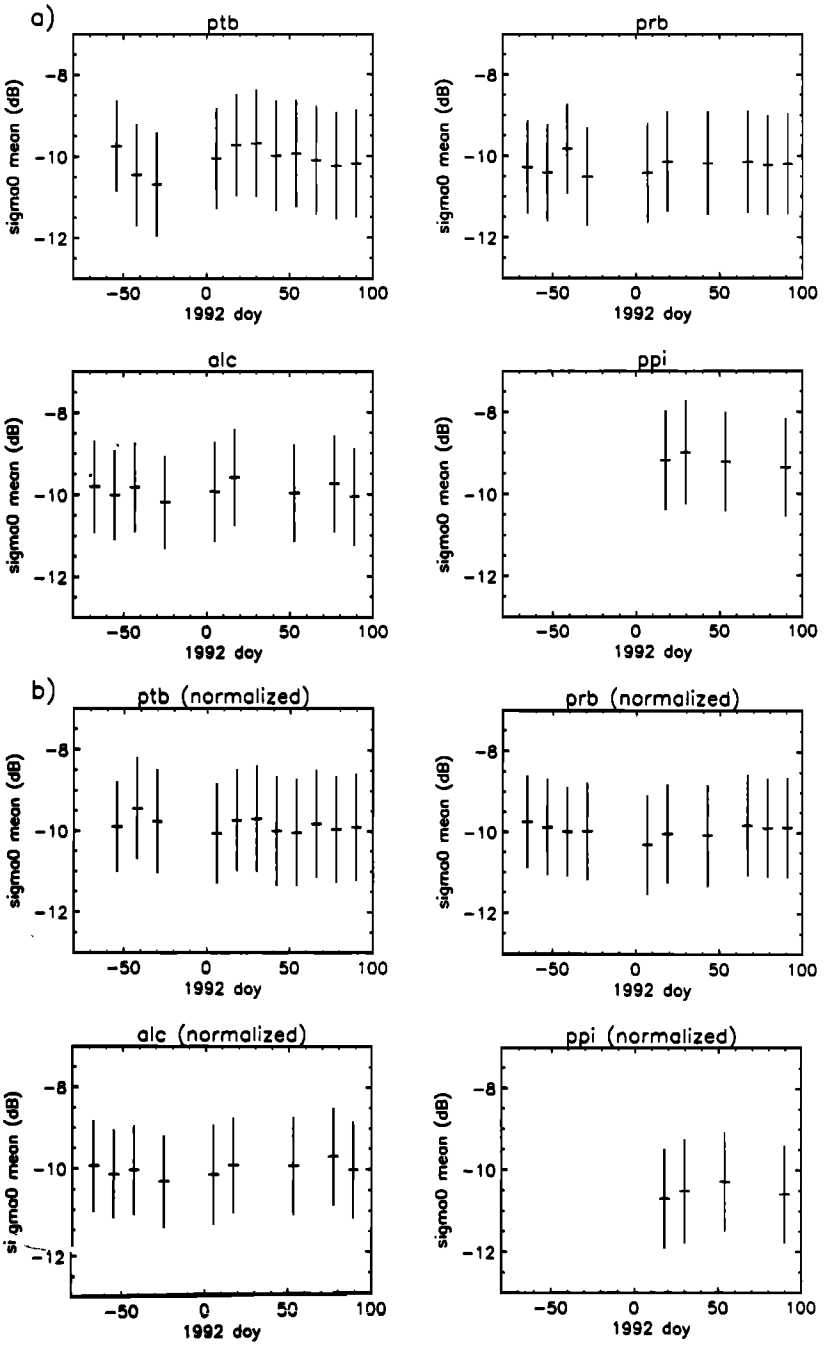

Figure 9. Temporal behavior of multiyear ice backscatter from the winter of 1991. (a) Plot of MY σ_0 versus time. (b) Plot of MY σ_0 versus time (after normalization of latitude backscatter dependence).

In both years there is a minimum at around 75°N in the western Beaufort Sea below which the backscatter trends higher. These higher values may reflect increased ice deformation, frequently observed in this region owing to the shear zone brought about by converging and diverging ocean currents [*Weeks et al.*, 1980]. As mentioned above, this observation may also result from the advection of the higher-backscatter MY sea ice from the eastern Beaufort. This effect is unexplained at this time.

The temporal behavior of MY backscatter from the winter of 1991–1992 is shown in Figure 9. These plots show the mean backscatter values from multiyear ice samples for all images within each orbit in the four tracks (sampled every 12 days). The plots show a fairly consistent signal with some variability in the earlier orbits. However, the data samples were taken at different latitudes in each orbit, thereby suggesting that the averages may be weighted by the latitudinal backscatter dependence. By taking the average latitude of the sampled pixels in each orbit an estimate of this variation can be made for each orbit from 1° binned values. After taking this variation into account the normalized mean backscatter values are shown in Figure 9b. Note the greater consistency of the signal in the earlier orbits. The overall signal has only slight variations and shows the multiyear ice to be a temporally stable backscatter target (with spatial variations) throughout this time period.

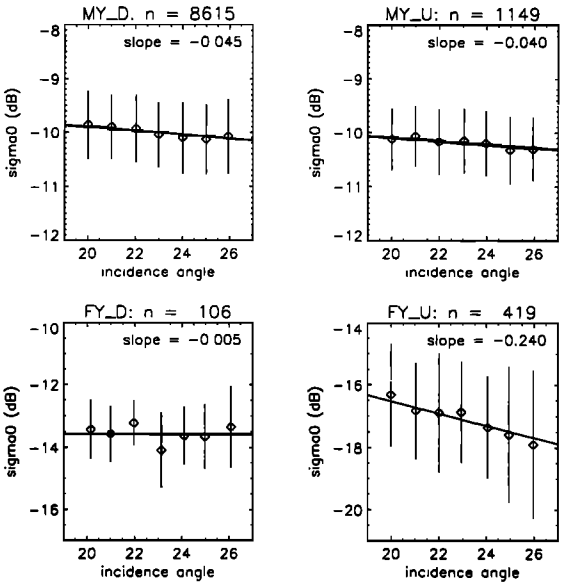

Figure 10. Incidence angle behavior of MY-D, MY-U, FY-D, and FY-U backscatter. The slope and number of points used in the regression are shown with each plot.

Comparison with scatterometer data. The multiyear ice backscatter observed here is approximately 1.5 dB lower than the C band scatterometer measurements of *Onstott* [1992]. Although within the absolute calibration uncertainty of the ERS-1 data products, this could be due to the resolution disparity between the ERS-1 SAR resolution element and the scatterometer footprint as mentioned earlier. Again, it is expected that SAR image backscatter observations are modulated to a higher degree by mixtures of ice types compared with scatterometer samples and that observations at the larger scale could be biased or have larger variance in backscatter than the pure ice type. The incidence angle dependence of the MY ice backscatter (decibel/degree of incidence angle) are derived from linear regressions of all the sample means. As expected, there is only a weak dependence on incidence angle over the range of incidence angles observed by ERS-1 as a result of the dominance of volume scattering. The slopes range from −0.03 to −0.1 dB/deg (see Figure 10) and are comparable to scatterometer observations.

4.2. Lead Ice

The histograms of the lead ice backscatter samples are shown in Figure 11. The lead ice samples give a mean of approximately −17 to −18 dB. The spatial and temporal variability of lead ice in the PIZ are shown in Figures 12 and 13. The arrangement of the plots is identical to those in Figures 5 and 9. A larger range of backscatter, approximately 3 dB, is seen compared to that observed for multiyear ice. We caution the reader again that we do not include leads with high backscatter (backscatter overlapping with that of MY and FY ice) owing to the difficulty in sampling these pixels because of the ambiguity of the signature of this ice type with the signature of MY and deformed FY ice. It has been shown [*Onstott*, 1992; *Steffen et al.*, 1992] that the backscatter of growing sea ice does not increase in a monotonic fashion. This is a limitation of our visual interpretation of image data with overlapping distribution of σ_0s.

The amount of variability can be attributed to the range of ice types that can exist in leads. The lead ice category covers a wide range of ice, with ages ranging from a few hours to possibly months. We reemphasize here that this category is defined geometrically and not by the age of the ice. Hence this large range of ice thicknesses, ages, and degree of deformation would promote a higher scatter in the values. It is also important to note that some of the lead ice signatures are close to the noise floor of the system. Because of this variability in the backscatter of lead ice (ice growth is continually altering the signatures), we did not explore and indeed did not observe any spatial and temporal trend in this ice type which contains a mixture of different types of ice. The temporal signatures (Figure 13), however, show that the mean of the samples observed here is fairly stable throughout the season and that there is a fairly high and consistent contrast between the MY and lead ice.

5. First-Year Ice Signature

Under cold winter conditions where the ice surface and snow cover are dry, the FY-D and FY-U ice types are visually discernible. The undeformed FY-U type has no major deformation features, while the FY-D type contains extensively ridged ice. The visual sampling of the backscatter statistics is based on this criterion. As discussed, the spatial sampling of deformed and undeformed first-year ice types is mostly restricted to the seasonal ice zones (below

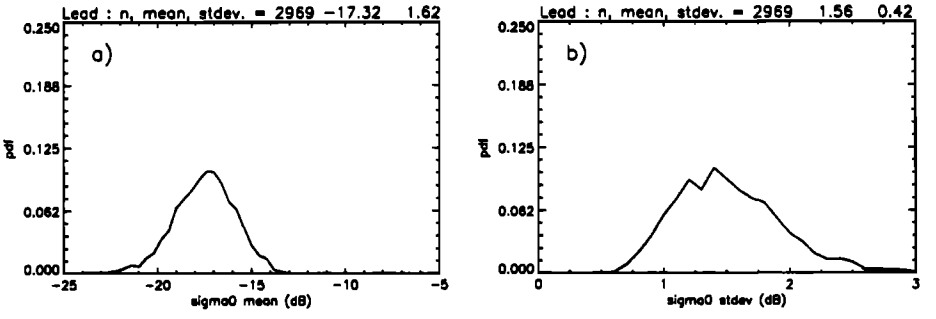

Figure 11. Histograms of mean and standard deviation of lead ice backscatter. (a) Histogram of mean backscatter of lead ice. (b) Histogram of standard deviation backscatter of lead ice data samples. Binning intervals are 0.4 dB and 0.1 dB for the mean and standard deviation plots, respectively. (n = number of points in data set; mean = mean backscatter in decibels; stdev = standard deviation in decibels.)

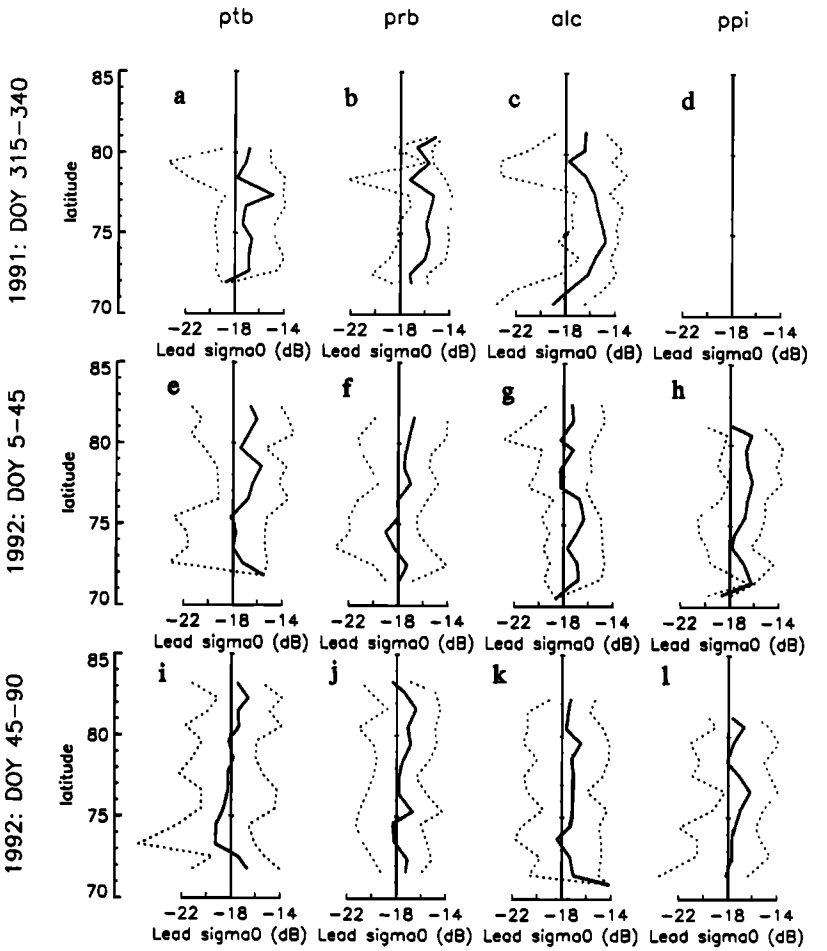

Figure 12. Spatial and temporal behavior of lead ice. The solid line in each plot shows the mean backscatter of all pixels within a 1° latitude bin plotted at their average latitude. The dotted lines show the minimum and maximum sample means found within that latitude bin. Bins are (a) ptb, 1991 DOY 315–340; (b) prb, 1991 DOY 315–340; (c) alc, 1991 DOY 315–340; (d) ppi, 1991 DOY 315–340; (e) ptb, 1992 DOY 5–45; (f) prb, 1992 DOY 5–45; (g) alc, 1992 DOY 5–45; (h) ppi, 1992 DOY 5–45; (i) ptb, 1992 DOY 45–90; (j) prb, 1992 DOY 45–90; (k) alc, 1992 DOY 45–90; (l) ppi, 1992 DOY 45–90.

75°) and thus have a significantly smaller number of samples (Table 2). Also, we would like to note here that the separation of these two ice types is more ambiguous owing to the seasonal nature of this ice. These ice types are not as stable, and their signatures tend to develop based on their thickness, deformation, and age. Because of this variability, there is little we can say about their spatial behavior and even less about the temporal behavior owing to our current inability to observe the signature evolution of the same FY ice floe for an extended period of time. The backscatter histograms for these two FY ice types are shown in Figure 14.

Deformed first-year ice. This deformed ice is usually associated with ridged and rafted ice where the backscatter is dominated by manifestations of this deformation. The mean backscatter of this ice type is approximately −14 dB and covers the range of σ_0 between MY ice and undeformed FY or lead ice (see Figure 14). The mean standard deviation of the samples is 1.2 dB. As expected, there is almost no dependence of the backscatter on incidence angle as a result of the deformed ice surface (see Figure 10). These observations are consistent with that of the scatterometer measurements of *Onstott* [1992].

Undeformed first-year ice. The undeformed first-year ice (FY-U) is also limited to lower latitudes. The mean backscatter of this ice type is approximately −17 to −18 dB, which is similar to the mean of the lead ice in the PIZ. The mean standard deviation of the samples is 1.6 dB. Figure 10 shows that the dependence of the backscatter on incidence angle is higher (0.15 dB/deg–0.37 dB/deg) than FY-D ice and MY ice, probably owing to the surface scatter contribution of a relatively undeformed and saline ice surface.

6. Summary

We have summarized the C band VV backscatter signatures of sea ice in the Beaufort Sea during the winter of 1991 and the early winter of 1992. The observations have shown that MY ice signatures, although temporally stable, vary within the region studied in this paper. The subtle spatial structure of MY ice backscatter signature in the Beaufort Sea can be observed because of the stability of the ERS-1 SAR sensor and the SAR image formation and calibration systems at the Alaska SAR Facility. The spatial structure of MY ice backscatter in the Beaufort Sea can be correlated to

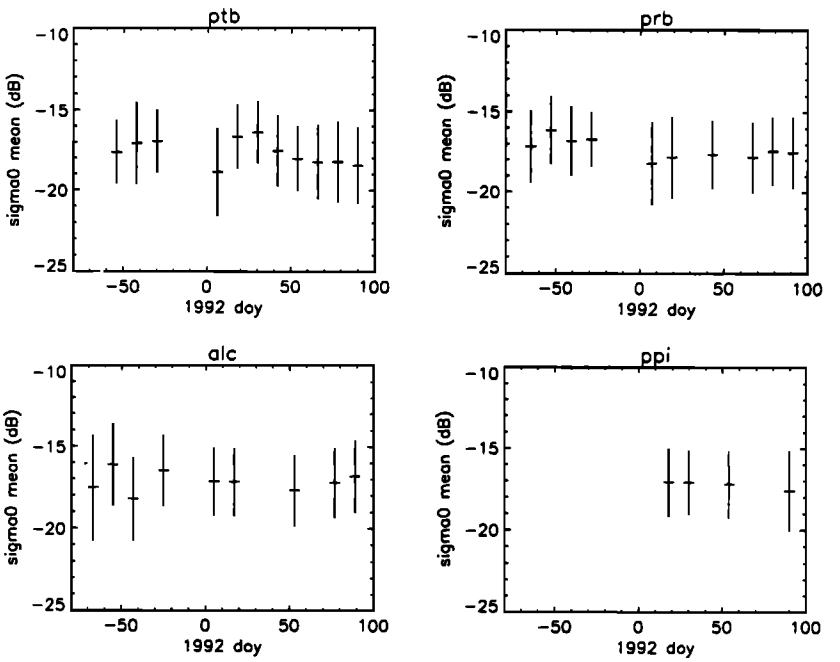

Figure 13. Temporal behavior of lead ice backscatter from the winter of 1991/1992.

physical processes, some of which are suggested in this paper. For example, the higher backscatter of MY ice near the Canadian Archipelago is an effect which could be caused by extensive pressure ridging due, in turn, to ice convergence at the land boundaries. We have speculated on the cause of this spatial structure in other regions, although observations do not exist to test these hypotheses. On the basis of MY ice signature observations from two winters this spatial structure remains substantially unchanged for this region. The spatial character of the backscatter of the MY ice cover contains physical information about its surface, volume, and deformation properties which can be related to atmospheric and oceanic forcings. These relationships should be explored and these spatial characteristics should be contrasted with other regions. We have also studied the range of backscatter of FY ice by sampling deformed and

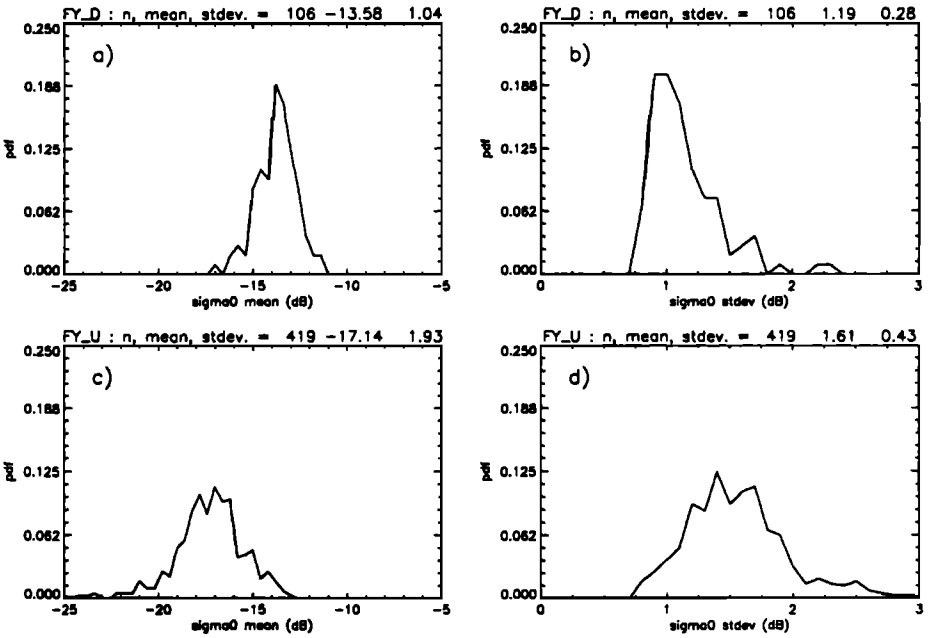

Figure 14. Histograms of mean and standard deviation of FY ice backscatter. (a) Mean backscatter of FY-D. (b) Standard deviation of backscatter of FY-D data samples. (c) Mean backscatter of FY-U. (d) Standard deviation of backscatter of FY-U data samples. Binning intervals are 0.4 dB and 0.1 dB for the mean and standard deviation plots, respectively. (n = number of points in data set; mean = mean backscatter in decibels; stdev = standard deviation in decibels.)

undeformed FY ice. Except for highly deformed FY ice, the FY ice signature also remains quite stable through the winter. Therefore the claim of consistent contrast between MY and FY ice during the winter season is borne out by the results shown here. Under these winter conditions the identification of principal ice types (MY and FY) can be done with relative ease. The lower backscatter ice in some of the frozen leads may be indicative of thinner ice types or of ice types with smooth surfaces, although observation of these ice types is limited by the type of radar data (single-frequency and polarization) and the method of data collection used here. Without in situ and other sensor observations, it remains a difficult task to unambiguously identify ice types other than the ones studied in this paper. We acknowledge that the shortcoming of our regional study is the lack of colocated data sets to support some of our observations. Colocated data sets with the spatial and temporal scale of our study are not available. Hence some of our interpretations remain speculative in nature. We have also limited our observations to a very small region of the Arctic in this paper. We intend to direct our attention to other areas (e.g., Chukchi Sea and E. Siberian Sea, etc.) in our future work.

Acknowledgments. The authors wish to thank F. Carsey, B. Holt, M. Drinkwater and S. Nghiem of JPL for their valuable comments on the manuscript and R. LeeJoice for compiling the data set for this study. This work was carried out at the Jet Propulsion Laboratory, California Institute of Technology under contract with the National Aeronautics and Space Administration.

References

Bourke, R., and A. S. McLaren, Contour mapping of Arctic Basin ice draft and roughness parameters, *J. Geophys. Res.*, *97*(C11), 17,715–17,728, 1992.

Carsey, F. D., Summer Arctic sea ice character from satellite microwave data, *J. Geophys. Res.*, *90*(C3), 5015–5034, 1985.

Cavalieri, D. J., B. A. Burns, and R. G. Onstott, Investigation of the effects of summer melt on the calculation of sea ice concentration using active and passive microwave data, *J. Geophys. Res.*, *95*(C4), 5339–5369, 1990.

Colony, R., Seasonal mean ice motion in the Arctic Basin, *Proc. of International Conference on the Role of the Polar Regions in Global Change*, pp. 290–300, University of Alaska, Fairbanks, 1990.

Colony, R., and A. Thorndike, Sea ice motion as a drunkard's walk, *J. Geophys. Res.*, *90*(C1), 965–974, 1985.

Drinkwater, M. R., LIMEX '87 ice surface characteristics: Implications for C-band SAR backscatter signatures, *IEEE Trans. Geosci. Remote Sens.*, *47*, 501–513, 1989.

Drinkwater, M., R. Kwok, D. Winebrenner, and E. Rignot, Multifrequency polarimetric SAR observations of sea ice, *J. Geophys. Res.*, *96*(C11), 20,679–20,698, 1991.

Fatland, R., and A. Freeman, Calibration and change detection of ASF/ERS-1 image data, in *IGARSS '92, International Space Year: Space Remote Sensing* (1164–1166, IEEE Press, New York, 1992.

Gow, A., S. A. Arcone, and S. G. McCrew, Microwave and structural properties of saline ice, CRREL Rep., pp. 20–87, Cold Reg. Res. and Eng. Lab., Hanover, N. H., 1987.

Gray, A. L., R. K. Hawkins, C. E. Livingston, L. D. Arsenault, and W. M. Johnstone, Simultaneous scatterometer and radiometer measurements of sea-ice microwave signatures, *IEEE J. of Oceanic Eng.*, *OE-7*(1), 20–32, 1982.

Holt, B., and S. A. Digby, Processes and imagery of first-year fast sea ice during the melt season, *J. Geophys. Res.*, *90*(C3), 5045–5062, 1985.

Kim, Y. S., R. K. Moore, R. G. Onstott, and S. Gogineni, Towards the identification of optimum radar parameters for sea-ice monitoring, *J. Glaciol.*, *31*(109), 214–219, 1985.

Kwok, R., E. Rignot, B. Holt, and R. G. Onstott, Identification of sea ice type in spaceborne SAR Data, *J. Geophys. Res.*, *97*(C2), 2391–2402, 1992.

Livingstone, C. E., and M. R. Drinkwater, Springtime C-band SAR backscatter signatures of Labrador Sea marginal ice: Measurements vs. modelling predictions, *IEEE Trans. Geosci. Remote Sens.*, *GE-29*(1), 29–41, 1991.

Livingstone, C. E., R. G. Onstott, L. D. Arsenault, A. L. Gray, and K. P. Singh, Microwave sea-ice signatures near the onset of melt, *IEEE Trans. Geosci. Remote Sens.*, *GE-25*(2), 174–187, 1987a.

Livingstone, C. E., K. P. Singh, and A. L. Gray, Seasonal and regional variations of active/passive microwave signatures of sea ice, *IEEE Trans. Geosci. Remote Sens.*, *GE-25*(2), 159–173, 1987b.

Lyden, J. D., B. Burns, and A. L. Maffet, Characterization of sea ice types using synthetic aperture radar, *IEEE Trans. Geosci. Remote Sens.*, *GE-22*(5), 431–439, 1984.

Onstott, R. G., SAR and scatterometer signatures of sea ice, in *Microwave Remote Sensing of Sea Ice*, *Geophys. Monogr. Ser.*, vol. 68, edited by F. D. Carsey et al., pp. 73–104, AGU, Washington, D. C., 1992.

Onstott, R. G., and S. P. Gogineni, Active microwave measurements of Arctic sea ice under summer conditions, *J. Geophys. Res.*, *90*(C3), 5035–5044, 1985.

Onstott, R. G., R. K. Moore, and W. F. Weeks, Surface-based scatterometer results of Arctic Sea ice, *IEEE Trans. Geosci. Electron.*, *GE-17*(3), 78–85, 1979.

Onstott, R. G., R. K. Moore, S. Gogineni, and C. V. Delker, Four years of low altitude sea ice broadband backscatter measurements, *IEEE J. Oceanic Eng.*, *OE-7*(1), 44–50, 1982.

Onstott, R. G., T. C. Grenfell, C. Matzler, C. A. Luther, and E. A. Svendsen, Evolution of the microwave sea ice signatures during early summer and midsummer in the marginal ice zone, *J. Geophys. Res.*, *92*(C7), 6825–6835, 1987.

Rignot, E., and M. R. Drinkwater, Winter sea ice mapping from multi-parameter SAR, *J. Glaciol.*, in press, 1994.

Shokr, M., Evaluation of second-order texture parameters for sea ice classification from radar images, *J. Geophys. Res.*, *96*(C6), 10,625–10,640, 1991.

Steffen, K., J. Heinrichs, J. Maslanik, and J. Key, Sea ice feature and type identification in merged ERS-1 SAR and Landsat thematic mapper imagery, in Proceedings of the First ERS-1 Symposium: Space at the Service of our Environment, *Eur. Space Agency Spec. Publ.*, *ESA SP-359*, 361–365, 1992.

Ulaby, F., R. K. Moore, and A. K. Fung, *Microwave Remote Sensing: Active and Passive*, vol. 3, Artech House, Norwood, Mass., 1986.

Wackerman, C. C., R. R. Jentz, and R. A. Shuchman, Sea ice type classification of SAR imagery, in Proceedings of IGARSS '88 Symposium, *Eur. Space Agency Spec. Publ.*, *ESA-SP 284*, 425–428, 1988.

Weeks, W. F., W. B. Tucker III, M. Frank, and S. Fungcharoen, Characterization of the surface roughness and floe geometry of sea ice over the continental shelves of the Beaufort and Chukchi seas, in *Sea Ice Processes and Models*, edited by R. S. Pritchard, pp. 283–299, University of Washington Press, Seattle, Wash., 1980.

Winebrenner, D. P., L. Tsang, B. Wen, and R. West, Sea-ice characterization measurements needed for testing of microwave remote sensing models, *IEEE J Oceanic. Eng.*, *OE-14*(2), 149–157, 1989.

G. F. Cunningham and R. Kwok, California Institute of Technology, 4800 Oak Grove Drive, MS300-235, Pasadena, CA 91190-8099.

(Received May 17, 1993; revised January 7, 1994;
accepted January 13, 1994.)